

Topological Phases in Triangular Lattices of Ru Adsorbed on Graphene: *ab-initio* calculations

C. Mera Acosta,^{1,*} Matheus P. Lima,^{1,†} R. H. Miwa,^{2,‡} Antônio J. R. da Silva,^{1,3,§} and A. Fazzio^{1,¶}

¹*Instituto de Física, Universidade de São Paulo, CP 66318, 05315-970, São Paulo, SP, Brazil*

²*Instituto de Física, Universidade Federal de Uberlândia, Uberlândia, MG, Brazil*

³*Laboratório Nacional de Luz Síncrotron, CP 6192, 13083-970, Campinas, SP, Brazil*

We have performed an *ab initio* investigation of the electronic properties of the graphene sheet adsorbed by Ru adatoms (Ru/graphene). For a particular set of triangular arrays of Ru adatoms, we find the formation of four (spin-polarized) Dirac cones attributed to a suitable overlap between two hexagonal lattices: one composed by the C sites of the graphene sheet, and the other formed by the surface potential induced by the Ru adatoms. Upon the presence of spin-orbit coupling (SOC) nontrivial band gaps take place at the Dirac cones promoting several topological phases. Depending on the Ru concentration, the system can be topologically characterized among the phases i) Quantum Spin Hall (QSH), ii) Quantum Anomalous Hall (QAH), iii) metal iv) or trivial insulator. For each concentration, the topological phase is characterized by the *ab-initio* calculation of the Chern number.

PACS numbers: 81.05.ue 73.43.Lp 31.15.A-

I. INTRODUCTION

The electronic properties of graphene can be tailored in a suitable way through the deposition of foreign atoms, allowing not only the development of electronic devices but also providing platforms for new physical phenomena¹⁻³. In particular, the adsorption of transition metals (TMs) on the graphene sheet (metal/graphene) has been considered as a promising route to modify the electronic properties of graphene. For instance, the control of spin-polarized current in graphene by the deposition of TMs (Mn, Fe Co and Ni)^{4,5}.

Recently, it was shown that it is possible to increase the Spin-Orbit Coupling (SOC) of graphene by depositing heavy atoms, such as indium and thallium⁶. In this case, the absence of net (local) magnetic moment preserves the time-reversal (TR) symmetry, giving rise to a Quantum Spin-Hall (QSH) state⁷ on the metal/graphene sheet with a nontrivial bulk band gap about three orders of magnitude greater than the predicted gap in pristine graphene. On the other hand, the majority of TMs with partially filled *d* orbitals, adsorbed on the graphene sheet, may promote a local net magnetic moment, and thus, will suppress the QSH state. However, based on the *ab initio* calculations, Hu *et al.* verified that such magnetic moment can be quenched by either applying an external electric field, or by a codoping processes, thus, recovering the QSH state⁸. They have considered ($n \times n$) periodic as well as random distributions of TM adatoms on the graphene sheet, and in both cases the QSH state was preserved. On the other hand, the appearance of a nontrivial energy bandgap in metal/graphene systems, due to the SOC and nonzero magnetic moment (breaking the TR symmetry), gives rise to the so called Quantum Anomalous Hall (QAH) effect⁹⁻¹². Furthermore, in a random distribution of TM adatoms on graphene sheet the SOC is not affected, and the intervalley *K* and *K'* scattering is somewhat suppressed¹³. That is, the nontriv-

ial topological phase of metal/graphene was preserved. Moreover, the tuning process of QAH effect, by application of external electric field, has been proposed¹⁴ for metal/graphene systems adsorbed with *5d* TMs.

Those findings allow us to infer that the electronic properties as well as the topological phases of metal/graphene systems can be controlled by means of a geometrical and chemical manipulation, as well as by application of external fields. In a recent experiment, Gomes *et al.*¹⁵ showed that it is possible to build up artificial graphene structures, so called “molecular graphene”, on solid surfaces by the manipulation of the surface potential. They have considered CO molecules forming a triangular lattice over the Cu(111) surface, CO/Cu(111). Such surface engineering allows a number of degrees of freedom to create of artificial lattices that exhibit a set of desirable electronic properties. For instance, the electronic properties of such “molecular graphene” can be tuned by changing the lateral distance between the CO molecules, by choosing another molecules instead of CO, or another surface instead of Cu(111). Indeed, recent works discuss the possibility of tuning the electronic properties of molecular graphene, as well as the realization of QSH state in CO/Cu(111) surfaces^{16,17}. Thus, it is experimentally possible to manipulate atoms and molecules in order to form an ordered array on top of a substrate. In the same sense, the usage of graphene as a substrate for adatoms or foreign molecules may also be interesting. In this case, the adatoms or molecules will be embedded in a two dimensional electron gas formed by the π orbitals of graphene.

In this work we performed an investigation of the interplay between the electronic properties and the geometry of Ru arrays adsorbed on the graphene sheet (Ru/graphene). We show that by changing the concentration of Ru adatoms it is possible to cover multiple topological phases¹⁸. Thus, with the same transition metal atom and the same triangular lattice structure, one

has in the lattice parameter (or TM separation) of this superstructure a dial that allows to tune the topological properties of the material.

The Ru adatoms, independently of their lattice geometry, strongly interact with graphene and locally modify the charge density at their neighboring carbon atoms. Due to the Ru \leftrightarrow Ru indirect interaction via graphene, the electronic structure of Ru/graphene system becomes ruled by the Ru lattice geometry. We have considered Ru adatoms forming triangular lattices with $(n \times n)$ periodicities, with respect to the graphene unitary cell, and according to the electronic structure we found three typical families of periodicities, showed in the Fig. 1. For $(3n \times 3n)$ periodicity, the Dirac cones are suppressed due to intervalley (K and K') scattering process, leading to a trivial bandgap. Whereas, for the both $((3n+1) \times (3n+1))$, and $((3n+2) \times (3n+2))$ there is a multiplicity of Dirac cones, and the appearance of a QAH phase. For these two last families, to better understand how the QAH phase emerges, we sequentially include the effects of an (i) electrostatic potential, (ii) an exchange potential, and (iii) the spin-orbit coupling. Considering only the electrostatic potential, two spin degenerated Dirac cones occur (at K and K') due to the presence of two overlapping hexagonal lattices, one composed by the C atoms of the graphene sheet, and the other composed by the surface potential on the graphene sheet induced (lying) by (on the barycenter of) the triangular lattice of the Ru adatoms. Upon inclusion of the exchange field, due to the net magnetic moment of Ru adatoms, there is a spin-splitting of all Dirac cones, leading to an amazing crossing between bands with reverse spin very close to the Fermi level. And finally, by turning on the SOC, the Rashba Spin-Orbit interaction couples the reverse-spin states leading to a non-trivial bandgap opening around the Fermi-level. Thus, the sum of the electrostatic potential, exchange field, and the SOC coupling leads to non-trivial topological phases in Ru/graphene systems.

We also show that the topological phase of the Ru/graphene systems changes for higher concentrations of Ru adatoms. Ru/graphene with the (2×2) periodicity presents a QSH phase, while for the (4×4) periodicity the system presents a metallic phase. The topological classification of the studied systems was made by the *ab-initio* calculation of the Chern number.

II. METHODOLOGY

All results presented in this work were obtained with first-principles calculations performed within the Density Functional Theory (DFT) framework¹⁹, as implemented in the SIESTA code²⁰. The Local Density Approximation (LDA)²¹ is used for the exchange-correlation functional. We used an energy cutoff of 410 Ry to define the grid in the real space, and the supercell approximation with a k-points sampling for the reciprocal space integration equivalent to $20 \times 20 \times 1$ in the unitary cell. The 2D

graphene sheets lie in the xy plane, and a vacuum of 20Å was used in the z-direction to avoid the undesirable interaction between the periodic images of graphene sheets. All the configurations of the Ru/graphene systems were fully relaxed until the residual forces on the atoms were smaller than 0.01 eV/Å.

In order to investigate the non-trivial topological phases in the Ru/graphene systems, we implemented the Spin-Orbit Coupling in the SIESTA code within the on-site approximation²². Within this approach, the Kohn-Sham Hamiltonian \mathbf{H} is a sum of the kinetic energy \mathbf{T} , the Hartree potential \mathbf{V}^H , the exchange and correlation potential \mathbf{V}^{xc} , the scalar relativistic ionic pseudopotential \mathbf{V}^{sc} , and the spin-orbit interaction \mathbf{V}^{SOC} . \mathbf{H} can be written as a 2×2 matrix in the spin space as:

$$\mathbf{H} = \mathbf{T} + \mathbf{V}^H + \mathbf{V}^{xc} + \mathbf{V}^{sc} + \mathbf{V}^{SOC} = \begin{bmatrix} \mathbf{H}^{\uparrow\uparrow} & \mathbf{H}^{\uparrow\downarrow} \\ \mathbf{H}^{\downarrow\uparrow} & \mathbf{H}^{\downarrow\downarrow} \end{bmatrix}. \quad (1)$$

All terms contribute to the diagonal elements, however only the \mathbf{V}^{xc} and the \mathbf{V}^{SOC} potentials have off-diagonal coupling terms due to the non-collinear spin. The spin-orbit matrix elements, as implemented in this work, are written as:

$$V_{ij}^{SOC} = \frac{1}{2} V_{l_i, n_i, n_j}^{SOC} \langle l_i, M_i | \mathbf{L} \cdot \mathbf{S} | l_j, M_j \rangle \delta_{l_i l_j}, \quad (2)$$

where $|l_i, M_j\rangle$ are the real spherical harmonics²³. The radial contributions $V_{l_i, n_i, n_j}^{SOC} = \langle R_{n_i, l_i} | V_{l_i}^{SOC} | R_{n_j, l_i} \rangle$ are calculated with the solution of the Dirac equation for each atom. The angular contribution $\mathbf{L} \cdot \mathbf{S}$, considering the spin operator in terms of the Pauli matrices, can be written as:

$$\mathbf{L} \cdot \mathbf{S} = \begin{bmatrix} L_z & L_- \\ L_+ & -L_z \end{bmatrix}. \quad (3)$$

The diagonal matrix elements for the SOC term $V_{ij}^{SOC, \sigma\sigma}$ (with $\sigma = \uparrow$ or \downarrow), are proportional to $\langle l_i, M_i | L_z | l_i, M_j \rangle$, which are different from zero only for $M_i = \pm M_j$. Thus, these terms couple orbitals with the same spins, and same $|M|$. On the other hand, the off-diagonal matrix elements $V_{ij}^{SOC, \sigma-\sigma}$ are proportional to $\langle l_i, M_i | L_{\pm} | l_i, M_j \rangle$, and thus couple orbitals with different spins and $M_i = M_j \pm 1$. These coupling terms could open bandgaps or generate the inversion of states that are essential to the physics of the topological insulators.

The band gaps were topologically characterized by calculating the Chern number (\mathcal{C}). This number is necessary to identify the topological class induced by the SOC in magnetic systems and is related to non-trivial Hall conductivity. In two dimensional systems the Chern number can be calculated within a non-Abelian formulation²⁴ by the following expression:

$$\mathcal{C} = \frac{1}{2\pi} \int_{BZ} \text{Tr}[\mathbf{B}(\mathbf{k})] d^2 k. \quad (4)$$

Where the trace is a summation over the band index, and only the occupied bands are taken in account.

The integration is done over the whole Brillouin Zone (BZ), and $\mathbf{B}(\mathbf{k})$ is a matrix representing the non-abelian momentum-space Berry curvature, whose diagonal elements can be written as²⁴:

$$\begin{aligned} B_n(\mathbf{k}) = & \lim_{\Delta_{k_y} \rightarrow 0} \lim_{\Delta_{k_x} \rightarrow 0} \frac{-i}{\Delta_{k_x} \Delta_{k_y}} \text{Im} \log [\langle u_{n\mathbf{k}} | u_{n\mathbf{k}+\Delta_{k_x}} \rangle \times \\ & \langle u_{n\mathbf{k}+\Delta_{k_x}} | u_{n\mathbf{k}+\Delta_{k_x}+\Delta_{k_y}} \rangle \langle u_{n\mathbf{k}+\Delta_{k_x}+\Delta_{k_y}} | u_{n\mathbf{k}+\Delta_{k_y}} \rangle \times \\ & \langle u_{n\mathbf{k}+\Delta_{k_y}} | u_{n\mathbf{k}} \rangle]. \end{aligned} \quad (5)$$

Where Δ_{k_x} (Δ_{k_y}) is the grid displacement in the k_x (k_y) direction of the reciprocal space, $|u_{n\mathbf{k}}\rangle$ is the cell-periodic Bloch functions in the (\mathbf{k}) point of the BZ, and n indicates the band index. This expression is quite adequate to perform calculations in systems with band crossing, and was implemented using a discrete grid in the reciprocal space.

III. RESULTS

The energetic stability of Ru adatoms on the graphene sheet was examined through the calculation of the binding energy (E^b) written as,

$$E^b = E[\text{graphene}] + E[\text{adatom}] - E[\text{Ru/graphene}].$$

$E[\text{graphene}]$ and $E[\text{adatom}]$ represent the total energies of the separated systems, graphene sheet and an isolated Ru atom, respectively, and $E[\text{Ru/graphene}]$ represents the total energy of the (final) Ru adsorbed graphene sheet, Ru/graphene. We have considered Ru/graphene systems with $(n \times n)$ periodicity with n ranging from 2 up to 12, thus, a set of different Ru concentrations on the graphene sheet. For the energetically most stable configuration, the Ru adatom presents a C_{6v} symmetry, sitting on the hollow site (H) of the graphene sheet. For the (4×4) periodicity, we obtained $E^b = 2.64$ eV at H , while the top site (above the C atom) is energetically less stable by 0.73 eV ($E^b = 1.91$ eV). There is a negligible dependence between the calculated binding energies and the Ru concentration. We did not find any energetically stable configuration for Ru adatoms on the bridge site (on the C-C bond). It is noticeable that the Ru binding energy is larger when compared with most of transition metals (TMs) adsorbed on graphene^{10,25,26}. At the equilibrium geometry the Ru adatom lies at 1.68 Å from the graphene sheet (vertical distance z), which is smaller when compared with most of the other TMs on graphene²⁶. Those findings allow us to infer that there is a strong chemical interaction between Ru adatoms and the graphene sheet. Indeed, our electronic structure calculations indicate that the Ru-4d orbitals, $d_{x^2-y^2}$, d_{xz} , d_{yz} and d_{yx} , are strongly hybridized with the carbon π (host) orbitals, while d_{z^2} behaves as lone pair orbitals.

Initially we will examine the electronic properties of Ru/graphene systems with $((3n+1) \times (3n+1))$ and $((3n+2) \times (3n+2))$ periodicities, which geometries are schematically represented in the panels (a) and (b) of Fig. 1, respectively. The $(3n \times 3n)$ [see Fig. 1(c)] systems will be discussed later on. Due to the Ru induced electrostatic field on the graphene sheet, the (5×5) Ru/graphene system exhibits two spin-degenerated band intersections (Dirac cones), at the K and K' points, separated by 0.78 eV [indicated as Δ_0 in Fig. 2(a)]. Further inclusion of spin polarization gives rise to a sequence of four spin-split band intersections, $C1 - C4$ in Fig. 2(b). The strength of the exchange field can be measured by the energetic separation E_x at the Γ point, of 0.66 eV, as shown in Fig. 2(b). In the same diagram, Δ_{C2-C3} indicates the energy separation between the highest occupied ($C3$) and lowest unoccupied ($C2$) Dirac cones. Notice that the linear energy dispersion (Dirac cones) has been preserved. Our calculated Projected Density of States (PDOS) [Fig. 2(c)] reveals that the Dirac cones are composed by similar contributions from C 2p (π orbitals) and Ru 4d orbitals. On the other hand, reducing the Ru adatom concentration by increasing the $(n \times n)$ periodicity, we find that, (i) the electronic contribution of Ru 4d orbitals to the Dirac cones $C2$ and $C3$ ($C1$ and $C4$) reduces (increases); (ii) in contrast, the C π orbitals contribution to $C1$ and $C4$ ($C2$ and $C3$) reduces (increases); (iii) the energy dispersions of the electronic bands that form the Dirac cones $C1$ and $C4$ have been reduced (becoming flatter). The localized character of Ru 4d orbitals will be strengthened, in accordance with (i). (iv) The electronic bands $C2$ and $C3$ retrieve the behavior of pristine graphene sheet, in accordance with (ii). The role played by the Ru adatom becomes negligible, and $\Delta_{C2-C3} \rightarrow 0$ for larger $(n \times n)$ periodicity, as shown in Fig. 2(d). In Fig. 2(e) we present the electronic band structure of (10×10) Ru/graphene, where (iii) and (iv) described above can be verified, and in Fig. 2(f) we present the expected picture of the electronic band structure of $(n \times n)$ Ru/graphene for $n \rightarrow \infty$. Those findings confirm the strong electronic coupling between the Ru adatoms and the graphene sheet (Ru \leftrightarrow graphene) leading to a long range interaction between the Ru adatoms via graphene (Ru \leftrightarrow Ru).

The total magnetic moment per Ru atom is also found to depend on the Ru coverage. Apart from the (2×2) periodicity which is non-magnetic, all studied structures present a finite magnetic moment. For all the $(3n \times 3n)$ periodicities the magnetic moment is $2.0\mu_B$. Whereas, for the $((3n+1) \times (3n+1))$ and $((3n+2) \times (3n+2))$ periodicities the magnetic moment increases with n from 1.75 to $2.0\mu_B$ at the limit of low coverage.

In order to improve our understanding on the role played by the (long range) Ru \leftrightarrow Ru electronic interaction, upon the presence of graphene host, we turned off such Ru \leftrightarrow Ru interaction by examining the electronic structure of a Ru adatom adsorbed on the central hexagon of a coronene molecule ($C_{24}H_{12}$), Ru/coronene. This

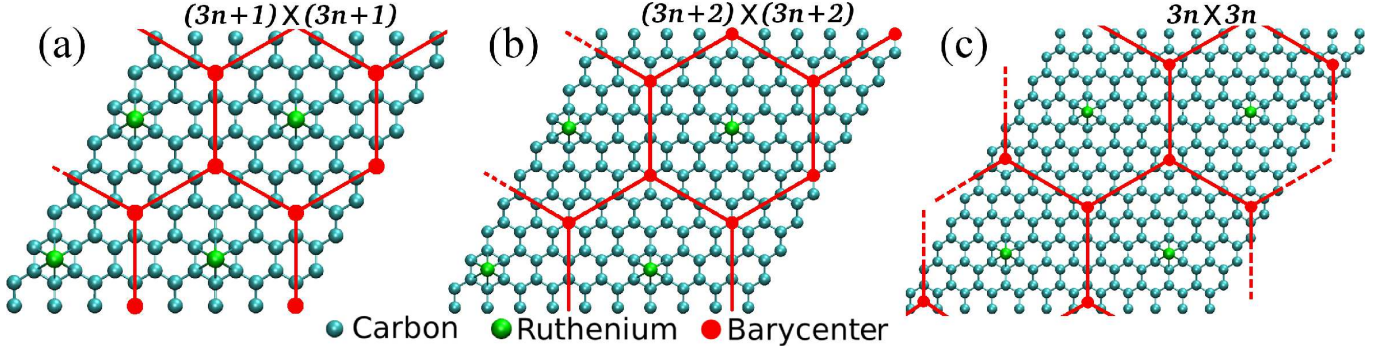


Figure 1. (Color online) Schematic representations of Ru/graphene systems with (a) (4×4) , (b) (5×5) and (c) (6×6) periodicities, respectively. These are examples of the $((3n+1) \times (3n+1))$, $((3n+2) \times (3n+2))$ and $(3n \times 3n)$ Ru/graphene systems, respectively. Here, n is an integer. The geometric centers of the triangles formed by the Ru adatoms (barycenters) form a honeycomb lattice, represented in the figure.

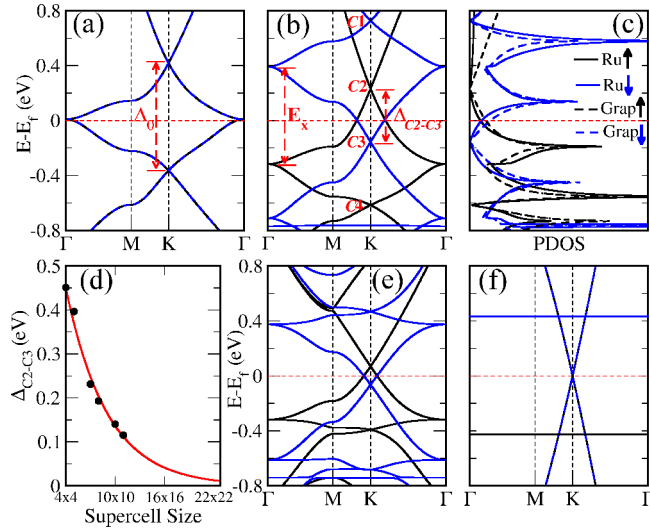


Figure 2. (Color online) Evolution of the electronic band structure of Ru/graphene with a (5×5) periodicity, considering successively the contributions of (a) electrostatic potential generated by Ru adatoms and (b) exchange field. In (c) is shown the PDOS of (b). Dark gray (Blue) and black lines are associated with the down and up spin, respectively. (d) Variation of the energetic separation, Δ_{C2-C3} , of the Dirac cones closer to the Fermi level ($C2$ and $C3$) relative to the concentration of Ru adatoms. (e) Band structure of (10×10) Ru/graphene system. (f) Expected picture of the band structure of $(n \times n)$ Ru/graphene systems with $n \rightarrow \infty$.

geometry is represented in the inset of Fig.3(a). This is a hypothetical system, since the equilibrium geometry of the Ru adatom in Ru/coronene is kept as the same as that obtained for the periodic Ru/graphene system. The calculated molecular spectrum, presented in Fig. 3(a), reveals that the HOMO and LUMO are both bi-degenerated states (mostly) composed by d_{xz} and d_{yz} orbitals of Ru adatom, being the spin-up (\uparrow) component for the HOMO and spin-down (\downarrow) for the LUMO. The

effect of $\text{Ru} \leftrightarrow \text{Ru}$ interaction, mediated by the graphene π orbitals, can be observed by comparing the panels (a) and (b) in Fig. 3. In Fig. 3(b), we present the electronic band structure of (4×4) Ru/graphene, where it is noticeable that the HOMO and LUMO energies of Ru/coronene compare very well with those of (4×4) Ru/graphene at the Γ point. We also identify the other $4d$ states (d_{z^2} , $d_{x^2-y^2}$ and d_{xy}). In the Ru/graphene system, the Ru $4d$ orbitals (hybridized with π orbitals of the graphene sheet) exhibit a dispersive character along the Γ -M and Γ -K directions within the Brillouin zone. We find that the Dirac cones with spin-up (spin-down) above (below) the Fermi level, indicated as $C2$ ($C3$) in Fig. 3(b), are formed by dispersive states with contributions of the d_{xz} , d_{yz} , $d_{x^2-y^2}$, and d_{xy} Ru orbitals. In other words, the states around the Fermi energy are composed by Ru orbitals with $l = 2$ and $m = \pm 1, \pm 2$, hybridized with the carbon p_z orbitals.

In Figs. 3(c) and 3(d) we present the Local Density of States (LDOS) of the Ru/coronene and (4×4) Ru/graphene systems, respectively. In those diagrams, the electronic states were projected onto a parallel plane to the Ru/coronene and Ru/graphene interfaces, 0.5 \AA above the molecule and the graphene sheet, respectively. We verify that the molecular spectrum of the HOMO and LUMO [Fig. 3(c)] are localized on the nearest neighbor (NN) and the next nearest neighbor (NNN) C sites of the Ru adatom, respectively. It is noticeable that for periodic Ru/graphene systems, regardless of the size and geometry of Ru adatoms, we have the similar electronic distribution for the occupied and empty states at the Γ point. *viz.*: the spin-up (spin-down) C π orbitals, localized on the NN (NNN) neighbor sites of the Ru adatom, contribute to the formation of the highest occupied (lowest unoccupied) states. Thus, we can infer that the Ru adatom locally defines the charge density both at its first and second nearest neighbor carbon atoms. On the other hand, due to the energy dispersion of those states along the $\Gamma \rightarrow K$ direction, the electronic states of the Dirac cone $C2$ will be mostly localized on the C atoms NN

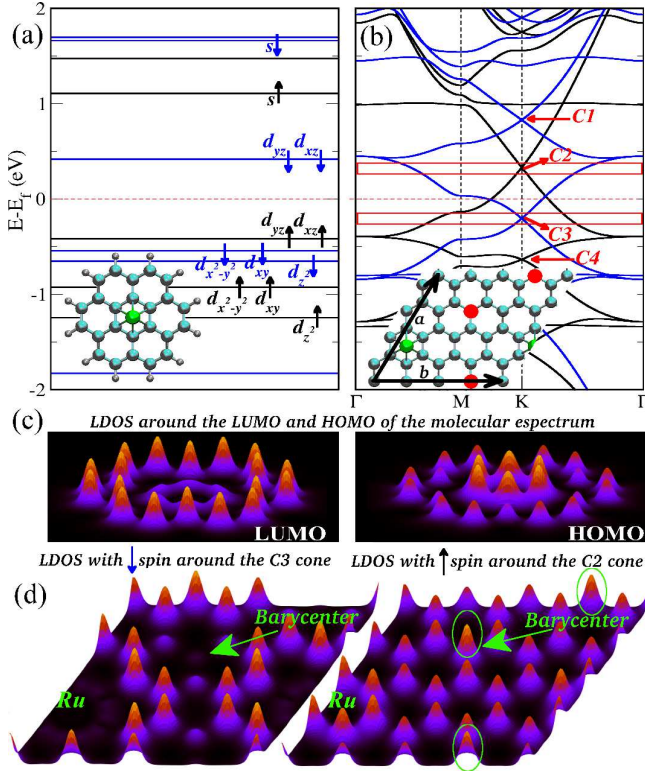


Figure 3. (Color online) Local effect of Ru adatom. (a) Molecular spectrum of Ru adsorbed on the coronene molecule, as illustrated in the structure at the bottom left of the box. (b) Electronic band structure of (4×4) Ru/graphene system without spin orbit coupling. The (red) boxes around C2 and C3 indicate the energy intervals used to calculate the LDOS. In the bottom left is represented the structure of the unit cell used. We indicate the barycenters with (red) balls. (c) LDOS around the LUMO (left) and HOMO (right) of molecular spectrum in arbitrary units. (d) LDOS with down and up spins around the C3 and C2 cones, respectively. We point out a C site associated with a barycenter, which is indicated in the structure in (b).

to the Ru adatoms [Fig. 3(d-right)], while the C atoms NNN to the Ru adatom [Fig. 3(d-left)] will contribute to the formation of C3. In addition, as shown in Fig. 3(d), not only the C atoms NN and NNN to the Ru adatom contribute to the formation of the Dirac cones, but also there are electronic contributions from the other C atoms of the graphene sheet. In particular, the LDOS of C2 exhibits a constructive wave function interference (LDOS peak) on the carbon atom lying at the geometric center of the triangular array of Ru adatoms, called hereafter as barycenter [indicated by an arrow in Fig. 3(d)], while it becomes destructive for the Dirac cone C3 [Fig. 3(d-left)].

Further LDOS calculations reveal that the other Dirac cone above E_F , C1 (spin-down), presents similar electronic distribution as compared to C2, whereas the LDOS of the Dirac cone C4 (spin-up), below E_F , is similar to that of C3. We find the same LDOS picture for the (7×7) and (10×10) Ru/graphene systems,

namely, the Dirac cones above E_F present LDOS peaks (i) on the NN C atoms to the Ru adatom and (ii) on the C atom localized at the barycenter of the triangular array of Ru adatoms. While the LDOS of the Dirac cones below E_F are (iii) localized on the NNN C atoms to the Ru adatoms, and (iv) present a negligible electronic contribution from the barycenter C atom. Such electronic picture, as described in (i)–(iv), is verified for the other $((3n + 1) \times (3n + 1))$ family of Ru/graphene systems, where the barycenter and the NN C sites to the Ru adatom belong to the same sublattice. Meanwhile, for the $((3n + 2) \times (3n + 2))$ Ru periodicity, such as (5×5) , (8×8) , and (11×11) Ru/graphene systems, the barycenter and the NNN C sites to the Ru adatom belong to the same sublattice. Such difference gives rise to a distinct LDOS picture for the Dirac cones. In Fig. 4(a-left) and 4(b-right) we present the LDOS for the (5×5) Ru/graphene, for the spin-up Dirac cone C2 and spin-down Dirac cone C3, above and below E_F , respectively. Here, compared with the (4×4) counterpart, in the (5×5) Ru/graphene system the Dirac cones above E_F obey (i) and (iv), whereas the Dirac cones below E_F are characterized by (ii) and (iii). Thus, we can infer that the electronic states at the barycenter C atom contributes to the formation of the Dirac cones below E_F , for the $((3n + 2) \times (3n + 2))$ Ru periodicity, whereas in the $((3n + 1) \times (3n + 1))$ Ru/graphene systems, the barycenter C atom contribute to the formation of the Dirac cones above E_F . In the region of integration used to calculate the LDOS around the C2 cone (formed by bands with up spin), there are states with opposite spin, which are associated with the formation of the cone C3, as shown in Fig. 3 (b). These states, although located around 0.5 eV above the vertex of the cone C3, have a distribution of peaks in the LDOS [shown in Fig. 4 (a-right)] similar to that presented at the vertex of the cone C3 [shown in 4 (b-right)]. The same behavior occurs for the other Dirac cones (C1-C4). Thus, the pattern of peaks distribution is not a characteristic only of the vertex of the cones, but a characteristic of the entire energy band that forms the cones.

In contrast, the band structures of the $(3n \times 3n)$ Ru/graphene systems do not show Dirac cones. In this case, the K and K' points are folded into the Γ point, and upon the presence of Ru adatoms in a $(3n \times 3n)$ periodicity, those electronic states face an intervalley scattering process suppressing the formation of the Dirac cones¹⁰. Figure 5(a) presents the electronic band structure of a (6×6) Ru/graphene system, where we find an energy gap of 0.11 eV at the Γ point. In this case, we find a quite different LDOS distribution [Fig 5(b)] on the graphene sheet, when compared with the other $((3n + 1) \times (3n + 1))$ and $((3n + 2) \times (3n + 2))$ Ru/graphene systems. Namely, the highest occupied (spin-up) states, at the Γ point, spread out somewhat homogeneously on the graphene sheet. Similar results (not shown) are found for the lowest unoccupied (spin-down) states, as well as for other $(3n \times 3n)$ periodicities. We find no LDOS peaks in the

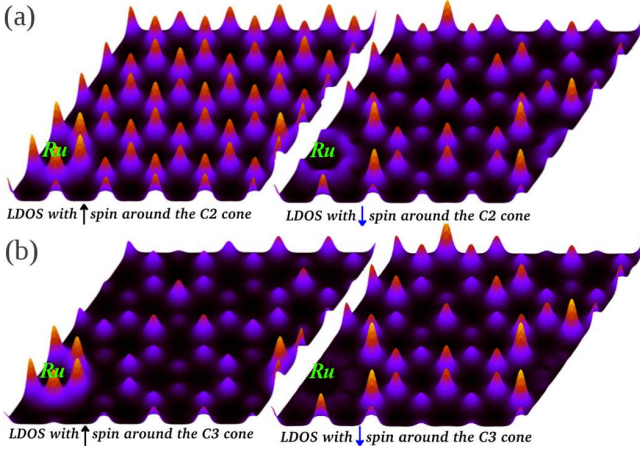


Figure 4. (Color online) LDOS for up and down spins around the energy level at which the (a) $C2$ and (b) $C3$ cones are formed for the (5×5) Ru/graphene system.

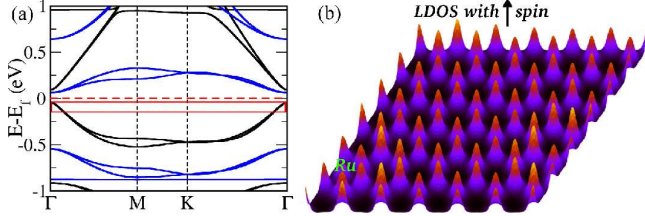


Figure 5. (Color online) (a) Electronic band structure and (b) LDOS for the (6×6) Ru/graphene system. The region of integration used to make the LDOS is represented by the (red) box in (a).

hexagonal lattice of barycenters, which can be attributed to the absence of carbon atoms, since for such Ru periodicity the barycenters lie at the hollow site of the graphene sheet.

In order to provide further support to such subtle compromise between the arrangement of the Ru adatoms on the graphene sheet and the formation of the Dirac cones, we have examined two additional configurations for Ru adatoms on graphene. That is, Ru adatoms forming rectangular and hexagonal lattices. For those Ru/graphene systems, we find two (spin-polarized) Dirac cones, instead of the four ones present at the triangular deposition of Ru on graphene. The disappearance of two cones occurs since the surface potential induced by the Ru adatoms has no longer a hexagonal symmetry. Here, we conclude that the presence of four Dirac cones is constrained by the triangular arrangement of the Ru adatoms on the graphene host.

By turning on the SOC we have the ingredients necessary to look for topological phases in Ru/graphene systems. Since in pristine graphene the radial contribution of the SOC term is negligible, and both the spin and the orbital magnetic moments are quenched, the properties of Ru/graphene system are defined by the 4d Ru orbitals. In the energy range in which the Dirac cones $C1-C4$ are

formed, there are similar contributions coming from the C 2p (π) and the Ru 4d orbitals, as already discussed above. This Ru contribution will give rise to the SOC effects. We analysed the wave functions around the Fermi energy, and concluded that their coefficients present significant changes only close to band crossings. Thus, the SOC does not modify either the electronic configuration or the effective population of the 4d orbitals when compared to the case when only the spin polarization is included. Likewise, with the SOC the total energy of the system decreases only by 0.48 meV, so that the change in binding energy is negligible. The most relevant band crossings occur at the Dirac cones above and below the Fermi energy as well as right at the Fermi energy. The SOC will open gaps at these band crossings.

In order to understand how the inclusion of this interaction contributes to the formation of energy gaps, we separately studied the diagonal and off-diagonal contributions of $\mathbf{L} \cdot \mathbf{S}$ to \mathbf{V}^{SOC} [see eqs. (2) and (3)].

We find that the off-diagonal term breaks the degeneracies at the K point, opening gaps at the Dirac cones $C1-C4$. Without the SOC, the Dirac cones are formed by intersections of bands with the same spin, where the states have a unique non null component of the spinor. As previously discussed, these bands have contributions from the orbital angular momentum $l = 2$ (4d orbitals) with $m = \pm 1$ and ± 2 ($d_{x^2-y^2}$, d_{xz} , d_{yz} and d_{yx} orbitals), leading to non-null off-diagonal terms. Through the self-consistent-cycle, these off-diagonal terms generate wavefunctions with non null coefficients at the spinor component which was previously zero, and break the degeneracies at the Dirac cones, opening an energy gap.

We also find that the diagonal elements contribute to the opening of gaps at the Fermi level, in the vicinity of K and K' points (see Fig. 6(a)). In this case, there are two effects: (i) The exchange and correlation potential generates a non-collinear spin coupling term via $V^{xc, \sigma-\sigma}$; and (ii) the splitting of the energy bands with opposite spins is generated by the addition (subtraction) of the matrix element $\langle l_i, m_i | L_z | l_j, m_j \rangle$ in $H_{ij}^{\uparrow\uparrow}$ ($H_{ij}^{\downarrow\downarrow}$). The addition of these two effects leads to the opening of gaps at the Fermi energy.

In Fig. 6 (a) we present the electronic band structure of the (5×5) Ru/graphene system. The SOC gives rise to energy gaps of 9.5 meV right at the points where the different spin band cross, characteristic of the QAH phase⁶ as depicted in Fig. 6 (b). In Fig. 6 (a) the spin texture is indicated, and is characteristic of a QAH topological phase. Also, we calculated the Chen number with the Eq. 4, obtaining $\mathcal{C} = -2$ for the (5×5) Ru/graphene, unequivocally confirming the QAH phase.

As discussed above, the electronic properties of Ru/graphene system, such as the strength of the exchange field (E_x), the energy separation between the Dirac cones (Δ_{C2-C3}), and the electronic contribution of Ru 4d to the formation of the Dirac cones $C1-C4$, all depend on the Ru concentration and $(n \times n)$ periodicity. In this work we also found an intriguing dependence be-

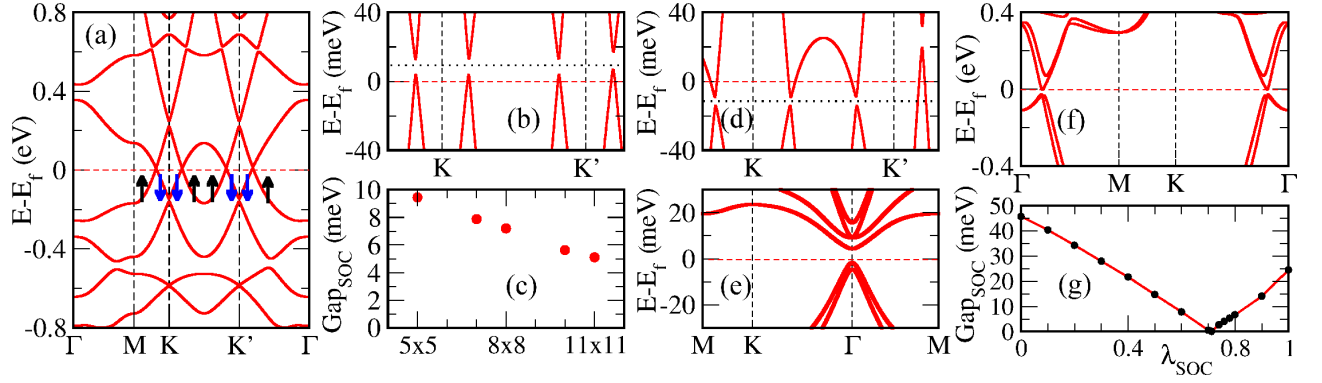


Figure 6. (Color online) The SOC effects in Ru/graphene systems. (a) Electronic band structure for the (5×5) periodicity with SOC. (b) Band structure of (a) near the Fermi level. (c) Energy band gaps for the $((3n+1) \times (3n+1))$ and $((3n+2) \times (3n+2))$ families with periodicities 5×5 or larger. Band structures for the (d) (4×4) , (e) (6×6) and (f) (2×2) periodicities. (g) Band gap variation of (f) with the SOC strength λ_{SOC} . The dashed (red) lines indicate the Fermi levels, whereas the black dotted lines is just to better visualize the energy gap.

tween the topological phase and the $(n \times n)$ periodicity of Ru/graphene. Indeed, by calculating the Chern number we found $\mathcal{C} = -2$ for all $((3n+1) \times (3n+1))$ and $((3n+2) \times (3n+2))$ Ru/graphene systems with periodicities 5×5 or larger. For those systems, the non-trivial band gap vary with the periodicity as shown in Fig 6 (c). On the other hand, for the (4×4) Ru/graphene system, the Ru \leftrightarrow Ru interaction is strengthened, and the Ru $4d$ orbitals become less localized. For this periodicity, with the SOC turned off the crossings between the up and down bands are not all aligned in energy, and with the SOC turned on the opening of gaps occurs at different energies, leading to a non-gapped band structure (metallic states), as shown in Fig. 6 (d). These metallic states prevent the observation of the QAH effect. However, we obtain a non-null Chern number ($\mathcal{C} \approx 0.98$), indicating a finite Anomalous Hall Conductivity, which is given by: $\sigma_{xy} = \mathcal{C} \frac{e^2}{h}$. For all the $(3n \times 3n)$ Ru/graphene systems we find $\mathcal{C} = 0$. This is a consequence of the trivial bandgap at the Γ point, generated by the intervalley K and K' scattering process [the band is shown in Fig. 6 (e)]. Thus, all the $(3n \times 3n)$ Ru/graphene systems are trivial insulators since the SOC is not strong enough to reverse the trivial band gap. Further increase on the Ru concentration (0.25 ML of Ru adatoms) was examined by considering the (2×2) periodicity. In these systems, the barycenters are located at the NNN C sites to the Ru adatoms. The (2×2) Ru/graphene exhibits quite different electronic and topological properties in comparison with the other Ru/graphene systems, because: (i) it presents an energy band gap, and zero net magnetic moment [see Fig. 6 (f)]; (ii) it presents the QSH phase. Here, we use the adiabatic continuity argument to prove (ii). This argument has been used to identify 2D and 3D topological insulators^{27–33}. According to this argument, if the Hamiltonian of a system is adiabatically transformed into another, the topological classification of the two systems can only change if the band gap closes. Thus, we

Table I. Multiple topological phases in Ru/graphene systems as a function of the periodicity.

periodicity	topological phase
(2×2)	QSH
(4×4)	metal
$((3n+1) \times (3n+1))^a$	QAH
$((3n+2) \times (3n+2))^b$	QAH
$(3n \times 3n)^b$	trivial insulator

^a for $n \geq 2$

^b for $n \geq 1$

smoothly changed the SOC strength by placing a multiplicative factor, λ_{SOC} , in the term associated with the on-site approximation of the SOC Hamiltonian, H_{SOC} . When this parameter is varied from zero to one, we observed a variation of the gap as shown in Fig. 6(g). At $\lambda_{SOC} = 0.712$ we find a metallic state (gap closing), generated by an inversion of the states that contribute to the formation of the HOMO and LUMO, indicating a transition from one trivial topological state (without SOC, $\lambda_{SOC} = 0$) to the QSH state (with SOC, $\lambda_{SOC} = 1$).

The above description is summarized in Table I, where can be appreciated the multiple topological phases exhibited by the Ru/graphene systems.

IV. SUMMARY

In summary, based on *ab initio* calculations, we investigate the structural and the electronic properties of graphene adsorbed by Ru adatoms, Ru/graphene. We map the evolution of the electronic charge density distribution around the Fermi level as a function of different Ru/graphene geometries. We found that the Ru adatom fixes the wave function phase of its NN and NNN C

atoms, whereas the Ru \leftrightarrow Ru interaction, mediated by the π orbitals of the graphene sheet, gives rise to four spin-polarized Dirac cones for the $((3n+1) \times (3n+1))$ and $((3n+2) \times (3n+2))$ Ru/graphene systems. The electronic distributions of the states that form those Dirac cones are constrained by the periodicity of the Ru adatoms on the graphene host. For triangular arrays of Ru adatoms, four spin-polarized Dirac cones are generated by a suitable coupling between the electronic states of two hexagonal lattices, one composed by the carbon atoms of the graphene host, and the other attributed to the (barycenter) surface potential on the graphene sheet induced by the triangular lattice of Ru adatoms. For other geometries, hexagonal and rectangular, we have only two spin-polarized Dirac cones, while there are no Dirac cones for $(3n \times 3n)$ Ru/graphene. The inclusion of SOC promotes multiple topological phases when graphene is doped with triangular arrays of Ru. The topological phase in those systems depends on the periodicities (or concentration) of Ru adatoms on the graphene sheet. For a high coverage in the (2×2) periodicity (25%) of Ru adatoms the QSH phase is present, whereas for the $((3n+1) \times (3n+1))$ and $((3n+2) \times (3n+2))$ Ru/graphene systems the QAH phase

will be preserved even for low coverage of Ru adatoms (less than 1%). These results are summarized in the Table I.

Even though transition metals adatoms have been used before to obtain distinct non-trivial topological phases in graphene, in previous works it was always considered that distinct transition metals would provide distinct topological phases. However, we have shown that this is not necessarily so. The same transition metal can provide distinct topological phases, depending on the particular geometrical arrangement.

V. ACKNOWLEDGEMENTS

The authors would like to thank Prof. Shengbai Zhang for fruitful discussions. Also, we would like to thank the financial support by Conselho Nacional de Desenvolvimento Científico e Tecnológico/Institutos Nacionais de Ciência e Tecnologia do Brasil (CNPq/INCT), the Coordenação de Aperfeiçoamento de Pessoal de Nível Superior (CAPES), and the Fundação de Amparo à Pesquisa do Estado de São Paulo (FAPESP).

* acosta@if.usp.br

† mplima@if.usp.br

‡ hiroki@infis.ufu.br

§ jose.roque@lnls.br

¶ fazzio@if.usp.br

- ¹ A. C. Neto, V. Kotov, J. Nilsson, V. Pereira, N. Peres, and B. Uchoa, *Solid State Commun.* **149**, 1094 (2009), ISSN 0038-1098, URL <http://www.sciencedirect.com/science/article/pii/S0038109809001379>.
- ² K.-H. Jin, S.-M. Choi, and S.-H. Jhi, *Phys. Rev. B* **82**, 033414 (2010), URL <http://link.aps.org/doi/10.1103/PhysRevB.82.033414>.
- ³ T. O. Wehling, A. V. Balatsky, M. I. Katsnelson, A. I. Lichtenstein, and A. Rosch, *Phys. Rev. B* **81**, 115427 (2010), URL <http://link.aps.org/doi/10.1103/PhysRevB.81.115427>.
- ⁴ M. P. Lima, A. J. R. da Silva, and A. Fazzio, *Phys. Rev. B* **84**, 245411 (2011), URL <http://link.aps.org/doi/10.1103/PhysRevB.84.245411>.
- ⁵ T. O. Wehling, A. I. Lichtenstein, and M. I. Katsnelson, *Phys. Rev. B* **84**, 235110 (2011), URL <http://link.aps.org/doi/10.1103/PhysRevB.84.235110>.
- ⁶ C. Weeks, J. Hu, J. Alicea, M. Franz, and R. Wu, *Phys. Rev. X* **1**, 021001 (2011), ISSN 2160-3308, URL <http://link.aps.org/doi/10.1103/PhysRevX.1.021001>.
- ⁷ C. L. Kane and E. J. Mele, *Phys. Rev. Lett.* **95**, 226801 (2005), URL <http://arxiv.org/abs/cond-mat/0411737>.
- ⁸ J. Hu, J. Alicea, R. Wu, and M. Franz, *Phys. Rev. Lett.* **109**, 266801 (2012), ISSN 0031-9007, URL <http://link.aps.org/doi/10.1103/PhysRevLett.109.266801>.
- ⁹ Z. Qiao, S. A. Yang, W. Feng, W.-K. Tse, J. Ding, Y. Yao, J. Wang, and Q. Niu, *Phys. Rev. B* **82**, 161414 (2010), ISSN 1098-0121, URL <http://link.aps.org/doi/10.1103/PhysRevB.82.161414>.

- ¹⁰ J. Ding, Z. Qiao, W. Feng, Y. Yao, and Q. Niu, *Phys. Rev. B* **84**, 195444 (2011), ISSN 1098-0121, URL <http://link.aps.org/doi/10.1103/PhysRevB.84.195444>.
- ¹¹ Z. Qiao, H. Jiang, X. Li, Y. Yao, and Q. Niu, *Phys. Rev. B* **85**, 115439 (2012), ISSN 1098-0121, URL <http://link.aps.org/doi/10.1103/PhysRevB.85.115439>.
- ¹² C.-Z. Chang, J. Zhang, X. Feng, J. Shen, Z. Zhang, M. Guo, K. Li, Y. Ou, P. Wei, L.-L. Wang, et al., *Science* **320**, 1921 (2013).
- ¹³ H. Jiang, Z. Qiao, H. Liu, J. Shi, and Q. Niu, *Phys. Rev. Lett.* **109**, 116803 (2012), URL <http://link.aps.org/doi/10.1103/PhysRevLett.109.116803>.
- ¹⁴ H. Zhang, C. Lazo, S. Blügel, S. Heinze, and Y. Mokrousov, *Phys. Rev. Lett.* **108**, 056802 (2012), ISSN 0031-9007, URL <http://link.aps.org/doi/10.1103/PhysRevLett.108.056802>.
- ¹⁵ K. K. Gomes, W. Mar, W. Ko, and H. C. Manoharan, *Nature* **483**, 306 (2012), ISSN 0028-0836, URL <http://dx.doi.org/10.1038/nature10941>.
- ¹⁶ M. Polini, F. Guinea, M. Lewenstein, H. C. Manoharan, and V. Pellegrini, *Nature Nanotech.* **8**, 625 (2013).
- ¹⁷ P. Ghaemi, S. Gopalakrishnan, and T. L. Hughes, *Phys. Rev. B* **86**, 201406 (2012), URL <http://link.aps.org/doi/10.1103/PhysRevB.86.201406>.
- ¹⁸ S. Oh, *Science* **340**, 153 (2013).
- ¹⁹ K. Capelle, *Brazilian Journal of Physics* **36**, 1318 (2006).
- ²⁰ J. M. Soler, E. Artacho, J. D. Gale, A. García, J. Junquera, P. Ordejón, and D. Sánchez-Portal, *Journal of Physics: Condensed Matter* **14**, 2745 (2002).
- ²¹ J. P. Perdew and A. Zunger, *Phys. Rev. B* **23**, 5048 (1981).
- ²² L. Fernández-Seivane, M. A. Oliveira, S. Sanvito, and J. Ferrer, *J. of Phys.: Condens. Matter* **18**, 7999 (2006).
- ²³ M. A. Blanco, M. Flrez, and M. Bermejo, *J. Mol. Struct.: THEOCHEM* **419**, 19 (1997), ISSN 0166-1280, URL

- <http://www.sciencedirect.com/science/article/pii/S0166128009700185>
- ²⁴ A. A. Soluyanov and D. Vanderbilt, Phys. Rev. B **85**, 115415 (2012), URL <http://link.aps.org/doi/10.1103/PhysRevB.85.115415>.
 - ²⁵ H. Sevincli, M. Topsakal, E. Durgun, and S. Ciraci, Phys. Rev. B **77**, 195434 (2008), URL <http://link.aps.org/doi/10.1103/PhysRevB.77.195434>.
 - ²⁶ K. T. Chan, J. B. Neaton, and M. L. Cohen, Phys. Rev. B **77**, 235430 (2008), URL <http://link.aps.org/doi/10.1103/PhysRevB.77.235430>.
 - ²⁷ H. Lin, R. S. Markiewicz, L. A. Wray, L. Fu, M. Z. Hasan, and A. Bansil, Phys. Rev. Lett. **105**, 036404 (2010).
 - ²⁸ D. Xiao, J. Ding, and Y. Yao, Phys. Rev. Lett. **106**, 016402 (2011).
 - ²⁹ B. A. Bernevig, T. L. Hughes, and S.-C. Zhang, Science **314**, 1757 (2006).
 - ³⁰ L. Fu and C. L. Kane, Phys. Rev. B **76**, 045302 (2007), URL <http://link.aps.org/doi/10.1103/PhysRevB.76.045302>.
 - ³¹ J. C. Y. Teo, L. Fu, and C. L. Kane, Phys. Rev. B **78**, 045426 (2008).
 - ³² H.-J. Zhang, C.-X. Liu, X.-L. Qi, X.-Y. Deng, X. Dai, S.-C. Zhang, and Z. Fang, Phys. Rev. B **80**, 085307 (2009).
 - ³³ J. E. Padilha, L. Seixas, R. B. Pontes, A. J. R. da Silva, and A. Fazzio, Phys. Rev. B **88**, 201106 (2013).